energies

MDPI

Article

Remote Sensing for Monitoring Photovoltaic Solar Plants in Brazil Using Deep Semantic Segmentation

Marcus Vinícius Coelho Vieira da Costa [1,2], Osmar Luiz Ferreira de Carvalho [3], Alex Gois Orlandi [1,2], Issao Hirata [1], Anesmar Olino de Albuquerque [2], Felipe Vilarinho e Silva [1], Renato Fontes Guimarães [2], Roberto Arnaldo Trancoso Gomes [2] and Osmar Abílio de Carvalho Júnior [2,*]

[1] Superintendency of Information Technology, Brazilian Electricity Regulatory Agency, Brasília 70.910-900, Brazil; marcus.imagem@aneel.gov.br (M.V.C.V.d.C.); alexorlandi@aneel.gov.br (A.G.O.); issaohirata@aneel.gov.br (I.H.); felipesilva.imagem@aneel.gov.br (F.V.e.S.)
[2] Department of Geography, University of Brasília, Brasília 70.910-900, Brazil; anesmar@ieee.org (A.O.d.A.); renatofg@unb.br (R.F.G.); robertogomes@unb.br (R.A.T.G.)
[3] Department of Computer Science, University of Brasília, Brasília 70.910-900, Brazil; osmarcarvalho@ieee.org
* Correspondence: osmarjr@unb.br

Abstract: Brazil is a tropical country with continental dimensions and abundant solar resources that are still underutilized. However, solar energy is one of the most promising renewable sources in the country. The proper inspection of Photovoltaic (PV) solar plants is an issue of great interest for the Brazilian territory's energy management agency, and advances in computer vision and deep learning allow automatic, periodic, and low-cost monitoring. The present research aims to identify PV solar plants in Brazil using semantic segmentation and a mosaicking approach for large image classification. We compared four architectures (U-net, DeepLabv3+, Pyramid Scene Parsing Network, and Feature Pyramid Network) with four backbones (Efficient-net-b0, Efficient-net-b7, ResNet-50, and ResNet-101). For mosaicking, we evaluated a sliding window with overlapping pixels using different stride values (8, 16, 32, 64, 128, and 256). We found that: (1) the models presented similar results, showing that the most relevant approach is to acquire high-quality labels rather than models in many scenarios; (2) U-net presented slightly better metrics, and the best configuration was U-net with the Efficient-net-b7 encoder (98% overall accuracy, 91% IoU, and 95% F-score); (3) mosaicking progressively increases results (precision-recall and receiver operating characteristic area under the curve) when decreasing the stride value, at the cost of a higher computational cost. The high trends of solar energy growth in Brazil require rapid mapping, and the proposed study provides a promising approach.

Keywords: solar panel; deep learning; semantic segmentation

check for updates

Citation: Costa, M.V.C.V.d.; Carvalho, O.L.F.d.; Orlandi, A.G.; Hirata, I.; Albuquerque, A.O.d.; Silva, F.V.e.; Guimarães, R.F.; Gomes, R.A.T.; Júnior, O.A.d.C. Remote Sensing for Monitoring Photovoltaic Solar Plants in Brazil Using Deep Semantic Segmentation. *Energies* **2021**, *14*, 2960. https://doi.org/10.3390/en14102960

Academic Editors: Benedetto Nastasi and Jesús Polo

Received: 16 March 2021
Accepted: 12 May 2021
Published: 20 May 2021

Publisher's Note: MDPI stays neutral with regard to jurisdictional claims in published maps and institutional affiliations.

Copyright: © 2021 by the authors. Licensee MDPI, Basel, Switzerland. This article is an open access article distributed under the terms and conditions of the Creative Commons Attribution (CC BY) license (https://creativecommons.org/licenses/by/4.0/).

1. Introduction

Solar energy is one of the most promising renewable energy sources, being crucial for sustainable development in places with intense sunlight. Several studies have shown that solar energy systems allow for economic and efficiency gains, driven by technological and productive development that enables cost reduction to overcome technical barriers [1,2]. According to Sampaio and Gonçalez [3], the main advantages of solar energy systems are reliability, low costs of operation and servicing, low maintenance, a free energy source, clean energy, high availability, generation closer to the consumer, a low environmental impact, potential to mitigate greenhouse gas emissions, and noiselessness. In contrast, the main disadvantages are a high initial cost, large installation area, high dependence on technology development, and climatic conditions (solar irradiation). The benefits of solar technology provided an exponential increase in installed solar energy capacity between 1992 and 2020 [4,5]. This detected growth of solar energy was not foreseen in previous scenarios of the Intergovernmental Panel on Climate Change's fifth assessment report [6].

Creutzig et al. [7] considered that the cause of underestimating the potential of solar energy was rapid technological learning and political support only for specific technologies. In 2019, China led the Photovoltaic (PV) solar energy capacity, followed by the European Union and the United States of America, where together they hold more than 64% of the world's total capacity.

Brazil offers good prospects for net-zero carbon energy due to its abundance of renewable energies: hydropower, bioenergy, wind, and solar [8]. Hydroelectric power is the primary generator of electric energy in Brazil. However, thermal energy is still needed to supply domestic demand in periods of prolonged drought [9–12]. Therefore, the challenge is to increase renewable energy production to supply the growing energy demand due to population growth and new technologies. One problem is that hydroelectric expansion prospects are in the Amazon region, with substantial environmental restrictions, such as extensive areas of flooding by dam reservoirs, methane emissions, and ecological changes [13–16]. In addition, climate change scenarios in Brazil for the 2030s and 2080s predict a decrease in rainfall and an increase in temperature, resulting in a reduction in hydroelectric production and an increase in solar (slight) and wind (significant) energy potential [17]. Thus, national progress needs to intensify alternative energy sources such as combining wind and solar sources [18].

The Brazilian territory has a high solar incidence availability, with a vast area close to the equator and without significant variations in the day's solar duration [19]. The semi-arid region has the most significant aptitude for installing solar power plants [20–25]. Between the two solar energy generation technologies, the Brazilian government has initially prioritized PV instead of concentrated solar power [26]. In 1995, the Hydroelectric Company of San Francisco developed the first PV system connected to Brazil's grid in Recife [27]. The crisis in the Brazilian electric sector between the years 2013 and 2015 favored the decentralization and diversification of the electric matrix sources. Therefore, since 2014, Brazil's solar energy has experienced a substantial expansion, with the first projects for PV Plants being contracted by way of public auctions. In the second half of 2015, solar energy production and distributed generation marked an inflection of growth driven by regulations and adoption of incentive changes [28]. Despite the various barriers to the development of solar energy (technological, economic, sociocultural, managerial, environmental, and political) [29–34], the current strong growth in PV energy brings optimistic perspectives for the electricity sector. Barbosa et al. [35] demonstrate, by modeling, that PV solar energy in Brazil will reach more than 36% of total electricity in 2050. This rapid expansion is mainly due to technology development, reducing investment costs, increasing the PV Panels capacity, and other enterprise cost reductions [36]. Furthermore, energy security policies and the eco-label design for improving air quality, by reducing greenhouse gas emissions, also contribute to solar energy growth [37].

Moreover, in developing countries such as Brazil, the PV solar plants are vital for ensuring energy security. Thus, inspecting solar plant constructions is important in order to carry out effective public policies. In Brazil, the Brazilian Electricity Regulatory Agency (ANEEL) is responsible for regulating the installed capacity expansion and monitoring the powerplant construction progress [38]. However, the inspection is manual, which will increase in complexity over time, requiring laborious work with skilled professionals and high costs for fieldworks and technical analysis. According to the ANEEL database, the growth expectancy for PV solar plant energy is considerable. For 2021, 32 new ventures are expected, and more than 140 for 2022. Furthermore, sustainable energy sources (e.g., wind and solar) tend to have many ventures with low energy production, increasing the number of processes to evaluate, urgently requiring automatic processes.

Remote sensing data (aerial photography and satellite imagery) enable inspection periodically, and have been widely used in the electrical sector for effective maintenance of electrical lines [39–41], thermal monitoring from nuclear power plants [42–45], environmental changes from hydroelectric dams [46–49], and energy consumption using nighttime light satellite imagery [50–52], among others. In solar energy, many studies use remote sens-

ing images, such as solar energy estimates [53–56], solar power plant site selection [57–62], PV potential on building rooftops [63–66], and area estimation [67,68].

In automatic detection, Deep Learning (DL) emerges as a powerful method, especially in regards to computer vision problems using convolutional neural networks (CNN), due to its ability to process multi-dimensional arrays [69] with wide remote sensing applications [70–75]. Several reviews were carried out on the different DL methods, in which object detection, semantic segmentation, and instance segmentation were the most common approaches [76–78]. The method choice is highly dependent on the task objectives. When the main goal is to make a pixel-wise classification (as is the case with PV solar plants), semantic segmentation is a great alternative [79,80].

Previous studies in PV solar panel detection have shown promising results using the DL method, presenting very high accuracy. However, most studies consider urban PV panels using aerial or high-resolution satellite images [81–83], while PV solar plant mapping is still restricted [84]. This approach is an effective alternative to construction inspection, requiring periodic data and free satellite imagery. Previous studies on PV panel detection have not yet shown reasonable solutions for classifying large regions, and the use of mosaicking with sliding windows is a promising solution [85–87].

The primary motivation for this study is the development of a methodology based on remote sensing for the automatic monitoring of new installations of PV solar plants. In Brazil, the high growth of solar energy throughout the territory, with a continental dimension, prevents on-site inspection due to the financial and time cost, requiring the development of technological alternatives. Therefore, this research aims to evaluate the use of DL methods, representing the state of the art of computer vision, to identify and monitor PV solar power plants from ANEEL's database using Sentinel-2 images. This methodology represents an innovation for the management and monitoring of installed solar energy structures on the Brazilian territory, and similar research does not exist in the country to date.

2. Materials and Methods

The present research had the following methodological steps (Figure 1): (2.1) data preparation; (2.2) DL models; (2.3) DL accuracy analysis; (2.4) mosaicking; and (2.5) mosaicking accuracy analysis.

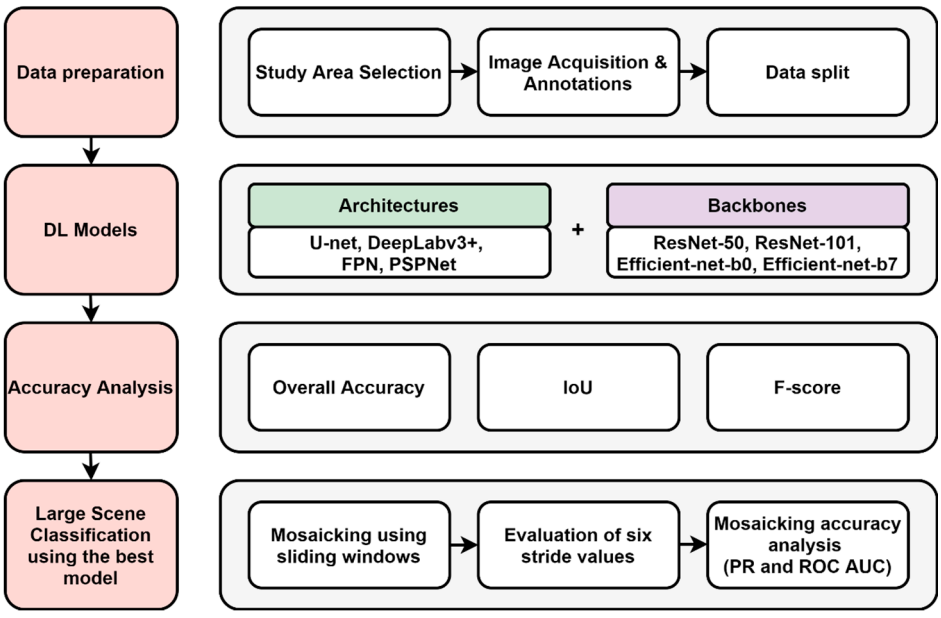

Figure 1. Methodological flowchart.

2.1. Data Preparation

2.1.1. Study Area

Brazil has a large and diverse territory, presenting different solar energy incidence [21]. Nevertheless, many areas are extremely suitable for the installation of PV panels. Therefore, we selected 24 areas to conduct this experiment (Figure 2). There are limited PV plants installed in the Brazilian territory and currently no open datasets considering Sentinel-2 data [88]. However, the development of methodologies and expansion of databases is a fundamental strategy for monitoring large-scale PV with a high growth trend.

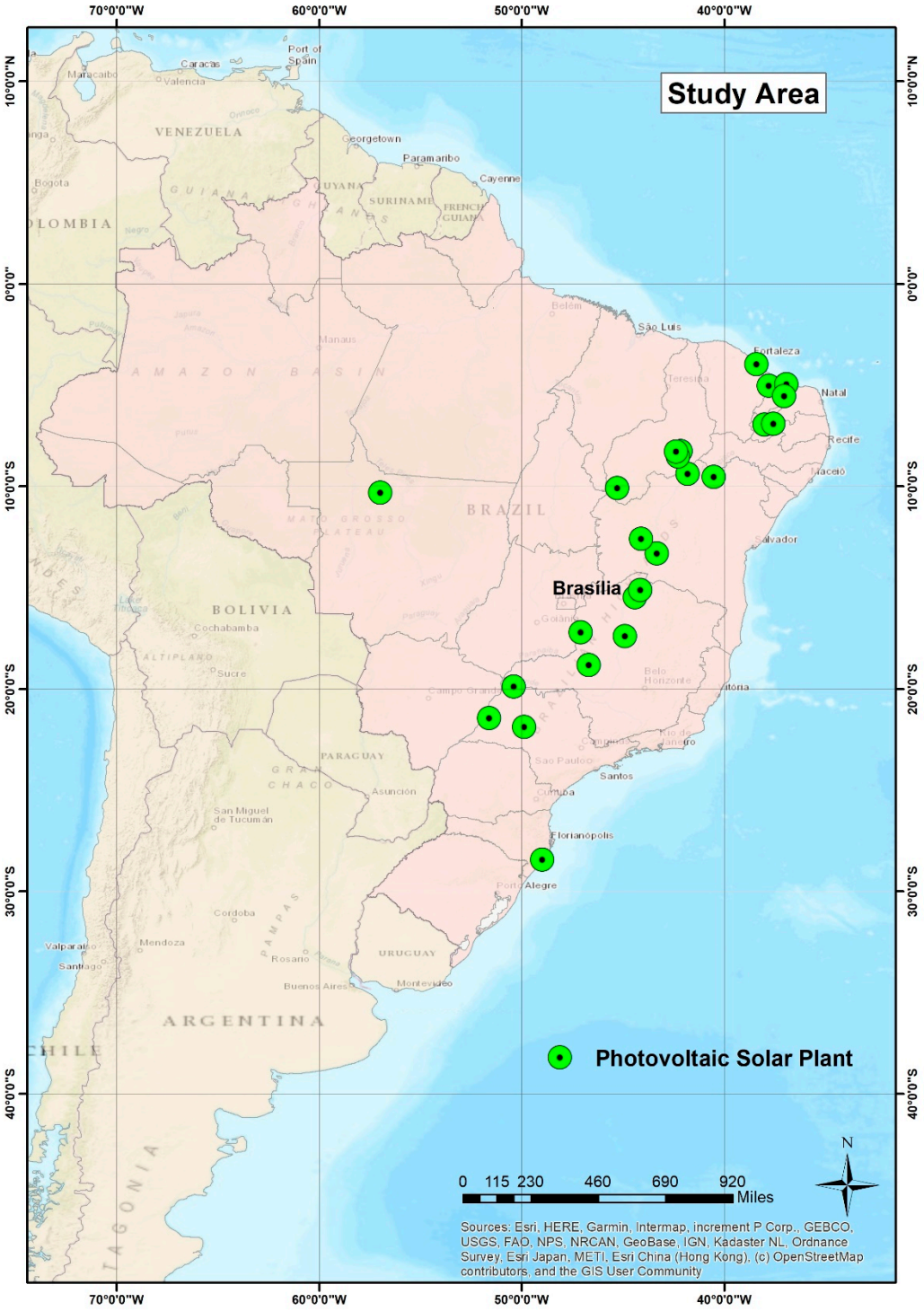

Figure 2. Study Area.

2.1.2. Image Acquisition and Annotations

We obtained Sentinel-2 cloudless images with four channels (Red, Green, Blue, and near infra-red) for each region containing PV solar power plants. For each image, a specialist manually annotated ground truth (GT) masks considering two classes: background and PV solar plant. The background class presents a wide variety of spectral behaviors, including the different soil and vegetation compositions present in a large-scale country such as Brazil. The research considered the difference in the light incidence and the construction of panels in each region for DL model training.

2.1.3. Data Split

After preparing each tile with their respective annotations, we separated the dataset into training, validation, and testing sets. For each area of interest that may contain more than one PV solar plant, we cropped at least seven 256 × 256-pixel tiles. Table 1 lists the distribution of areas and images for training, validation, and testing.

Table 1. Data split in training, validation, and test sets.

Set	Number of Areas	Number of Images
Train	15	210 (75%)
Validation	5	40 (14.28%)
Test	4	30 (10.71%)

2.2. DL Models

2.2.1. Architectures and Backbones

Semantic segmentation allows for a pixel-wise classification, being highly suitable for many remote sensing applications [74]. Most semantic segmentation networks include an encoder/decoder structure. The encoder aims to extract features, whereas the decoder restores the image's original dimensions. In the last few years, many architectures were proposed to increase performance in this task (e.g., U-net [89], SegNet [90], Feature Pyramid Network (FPN) [91], DeepLab [92,93], and Pyramid Scene Parsing Network (PSPNet) [94], and backbones (e.g., ResNet [95], ResNeXt [96], and Efficient-net [97]). This study evaluated four commonly used architectures (U-net, DeepLabv3+, FPN, and PSPNet) and four backbones (ResNet-50 (R-50), ResNet-101 (R-101), Efficient-net-b0 (Eff-b0), and Efficient-net-b7 (Eff-b7)). We used models from the Semantic Segmentation repository [98], which provides different architectures and backbones in Pytorch.

2.2.2. Model Configurations

In addition to choosing the appropriate models, it is crucial to make fine adjustments for the task at hand. The first problem is the reduced number of available samples. Therefore, in addition to obtaining at least seven frames from each location, we applied two augmentations in the training process: random horizontal flip and random vertical flip (both with a probability of 0.5). The second problem is class distribution (there are many more background pixels than solar panel pixels). Thus, we used a loss function that minimizes this effect, the Dice Loss:

$$\text{Dice Loss} = \frac{2x(\text{pred} \cap \text{GT})}{|\text{pred}| + |\text{GT}|}, \quad (1)$$

in which pred is the DL prediction, and GT is the ground truth mask. In addition, we used transfer learning with Imagenet [99] pre-trained weights for faster convergence; to avoid overfitting, we applied callbacks, saving the model with the lowest Dice Loss in the validation set. Regarding hyperparameters, we used: (a) 300 epochs; (b) Adam optimizer; (c) 5 × 10-3 learning rate (lr); and (d) batch size of 5.

2.3. DL Accuracy Analysis

Accuracy analysis is a fundamental step for DL model evaluation. Since semantic segmentation models provide a pixel-wise mask, the metrics compare the predicted mask and the GT mask through confusion matrix metrics. The confusion matrix (Table 2) has four quadrants in binary tasks: True Negatives (TN), True Positives (TP), False Positives (FP), and False Negatives (FN).

Table 2. Confusion matrix.

		Prediction	
		0	**1**
Ground truth	**0**	TN	FP
	1	FN	TP

The model outputs probability, whereas the GTs are integers. Thus, it was necessary to establish a cutoff point for the threshold metrics. A stricter threshold tends to reduce the commission errors, while a more permissive threshold tends to reduce omission errors. Thus, we applied a commonly intermediate threshold of 0.5 for three metrics (overall accuracy, F-score, and IoU):

$$\text{Overall Accuracy} = \frac{\text{TP} + \text{TN}}{\text{TP} + \text{TN} + \text{FP} + \text{FN}}, \quad (2)$$

$$\text{IoU} = \frac{\text{TP}}{\text{TP} + \text{FP} + \text{FN}}, \quad (3)$$

$$\text{F} - \text{score} = \frac{\text{TP}}{\text{TP} + \frac{1}{2}(\text{FP} + \text{FN})}, \quad (4)$$

2.4. Mosaicking

The 256 × 256 pixel tiles used in training may not represent an entire scene, requiring a postprocessing stage. Mosaicking using a sliding window algorithm is a very promising solution. However, combining frames side by side to reconstruct a scene may also induce errors in the single frame edges. A way to minimize this effect is to apply a sliding window with overlapping pixels, where the final pixel will be the average from the overlapped pixels. Thus, we compared six different stride values for the mosaicking strategy: 8, 16, 32, 64, 128, and 256 (adjacent frames). Figure 3 shows four images with consecutive frames using different stride values. The smaller the stride value, the more overlapping pixels (which tends to reduce errors in the frame edges).

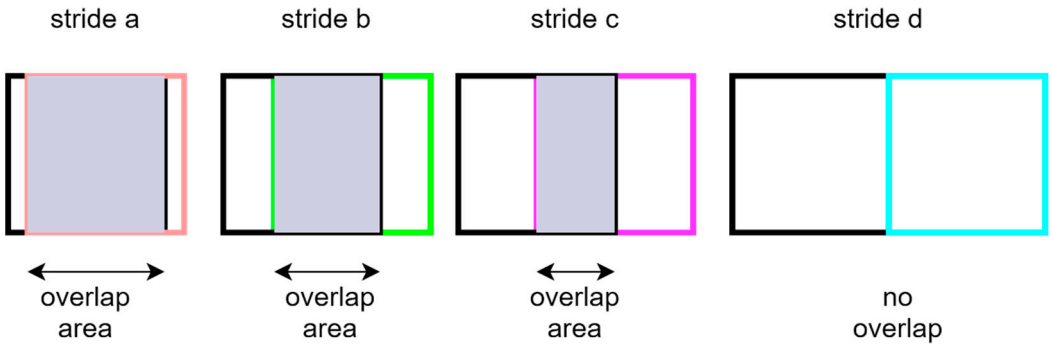

Figure 3. Four examples of different stride values of two consecutive frames in ascending order, where the stride value a < b < c < d.

2.5. Mosaicking Accuracy Analysis

To evaluate the mosaicking, we analyzed the ranking metrics Receiver Operating Characteristic Area Under the Curve (ROC AUC) and Precision-Recall (PR) AUC, considering six stride values: 8, 16, 32, 64, 128, and 256. The ROC curve considers the true positive rate ($TP/(TP + FN)$) and false positive rate ($FP/(TN + FP)$) and the PR curve considers the precision ($TP/(TP + FP)$) and recall ($TP/TP + FN$). From the points generated, it is possible to calculate the area under these curves.

3. Results

3.1. DL Metrics Results

Overall, the different architectures and backbones presented good results (Table 3). The U-net presented the best metrics results regarding the different architectures, followed by DeepLabv3+, FPN, and PSPNet. Despite the higher complexity of the DeepLabv3+ architecture, the U-net presented better results as the targets do not present a high variance in scaling, one of the most significant benefits of this model. Moreover, although PSPNet provided the worst results, the difference is not extremely large, and the training period is considerably lower (less than half the time to train the Eff-b7 using the U-net architecture, and nearly one-fifth of the period for training on the DeepLabv3+ architecture). When analyzing the different backbones, apart from Eff-b0 with the PSPNet architecture, the results did not change significantly. Moreover, metrics-wise, the accuracy score shows high values among all models (<3% variation), possibly due to the fact that there are many more pixels corresponding to the background class than the panels class. The IoU and F-score provide much more meaningful results. The Eff-b7 using the U-net architecture had the best IoU and F-score results, and an intermediate computational cost.

Table 3. Semantic segmentation evaluation (accuracy, IoU, F-score, and epoch period) using three architectures (U-net, DeepLabv3+, and PSPNet), and four backbones (Efficient-net-b7 (Eff-b7), Efficient-net-b0 (Eff-b0), ResNet-101 (R-101), and ResNet-50 (R-50)).

Architecture	Backbone	Accuracy (%)	IoU (%)	F-Score (%)	Epoch Period (s)
U-net	Eff-b7	98.08	91.17	95.38	12
	Eff-b0	98.05	90.97	95.27	5
	R-101	97.96	90.58	95.06	5
	R-50	97.98	90.70	95.12	4
DeepLabv3+	Eff-b7	97.83	89.98	94.73	26
	Eff-b0	97.77	89.82	94.64	5
	R-101	97.46	88.47	93.88	7
	R-50	97.02	86.63	92.84	6
PSPNet	Eff-b7	97.35	88.03	93.64	5
	Eff-b0	96.73	85.43	92.14	3
	R-101	97.06	86.98	93.04	3
	R-50	97.23	87.60	93.39	3
FPN	Eff-b7	97.38	87.99	93.61	12
	Eff-b0	97.45	88.21	93.73	5
	R-101	97.58	89.21	94.30	6
	R-50	97.25	87.74	93.47	5

Figure 4 shows three examples from the test set, and three examples from the validation set with their corresponding original images (RGB channels), GT, and prediction. Despite some errors in the edges of the objects, these results suggest a correct identification of the target, with few errors.

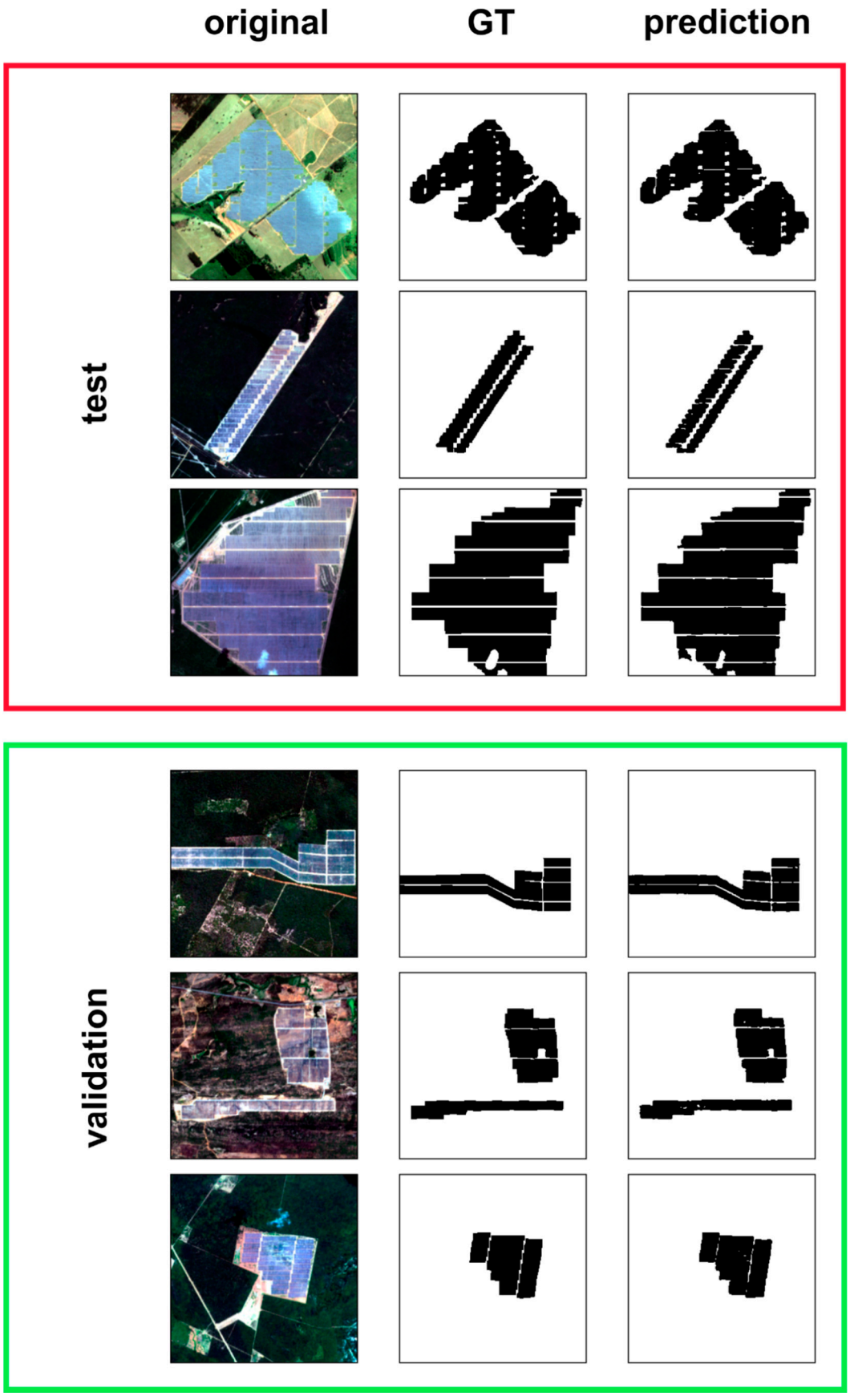

Figure 4. Three examples from the test set and three examples from the validation set with their corresponding original image, ground truth (GT), and prediction.

3.2. Mosaicking Results

Table 4 shows the ROC AUC scores using the 1536 × 768 area, using six different stride values (8, 16, 32, 64, 128, and 256). The analysis only considered the best model (U-net with Eff-b7 backbone). When the stride value decreases, results progressively improve in both metrics. Nevertheless, decreasing the stride value increases the computational cost needed, becoming a significant limitation, especially for practical applications.

Table 4. ROC AUC, PR AUC, and processing time for 8, 16, 32, 64, 128, and 256 stride values.

Stride	ROC AUC	PR AUC	Processing Time (s)
8	99.42	97.85	2829
16	99.25	97.56	734
32	98.89	96.99	193
64	98.66	96.42	63
128	98.36	95.39	15
256	98.16	94.49	4

Figure 5 shows the original image, its corresponding GT, and the prediction using U-net with Eff-b7 backbone and 8-pixel stride value on a 1532 × 768-pixel image. This mosaicking strategy enables the classification of areas with large dimensions, outputting images with no discontinuity.

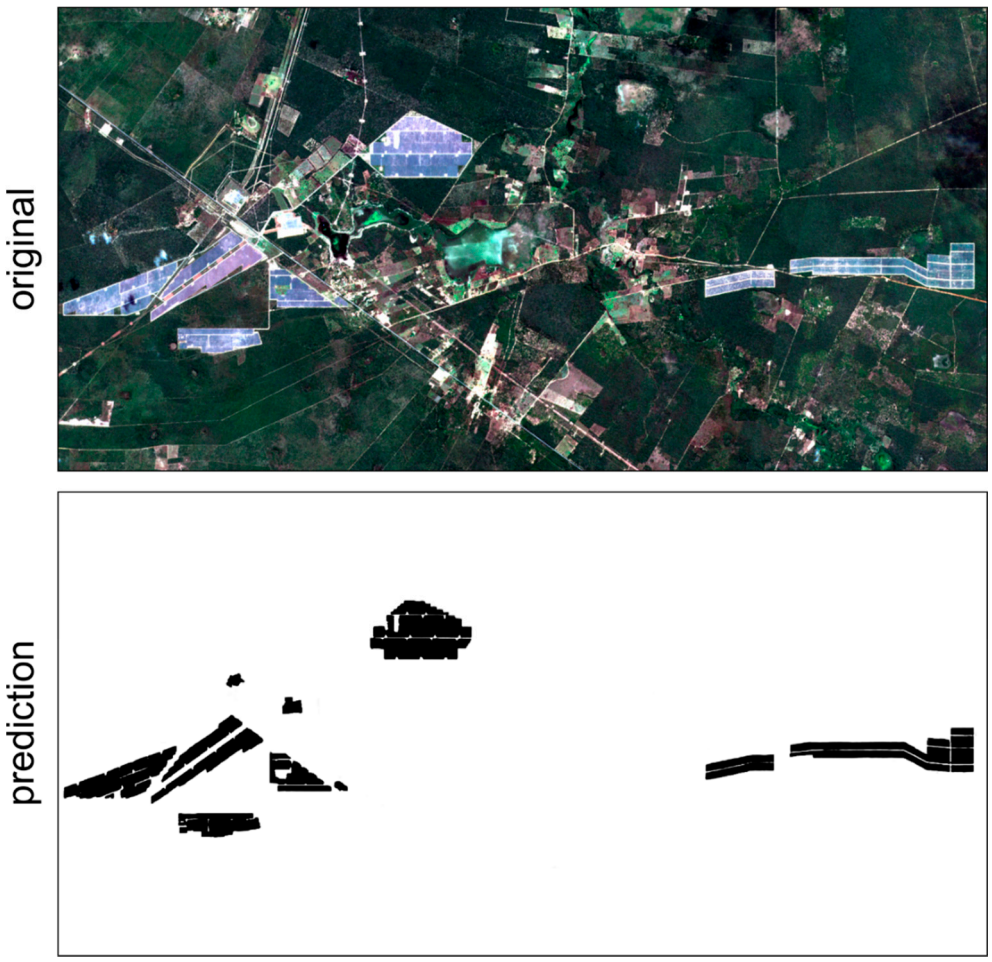

Figure 5. Mosaic representation on a 1536 × 768-pixel image with the original image, the corresponding ground truth (GT), and prediction using the U-net with Efficient-net-b7 backbone.

4. Discussion

The best result of our study was the U-net with the Eff-b7 backbone, although the other methods also reach high or adequate values. However, an unexpected result is that U-net outperformed DeepLabv3+ by a slight margin. This result is probably because the input images do not present multi-scale objects—one of the main contributions of the DeepLabv3+ method. Therefore, these results show that simpler structures may be well suited in some scenarios, highlighting the importance of testing different architectures.

Other solar panel detection studies using DL methods have demonstrated high accuracy in different locations. However, studies carried out on PV solar plants are still much lower than residential PV solar panels. Considering the large-scale solar plants, Hou et al. [84] proposed a study in China with one thousand images achieving 95% IoU from the U-net model. They used a much more significant amount of data, and the results were not dissimilar to ours (92% IoU).

Generally, accuracy results are lower in residential PV solar panels due to their smaller dimension and higher susceptibility to noise interference. Yuan et al. [100] applied a simple ConvNet for large-scale solar panel mapping from aerial images, and evaluated their model in the cities of Boston and San Francisco using completeness (0.84 and 0.87) and correctness (0.81 and 0.85) metrics. Yu et al. [101] proposed DeepSolar with a substantial amount of training data using high-resolution satellite images, obtaining 93.1% recall and 88.5% precision, results very similar to our F-score (95%). Zhuang et al. [83] applied the U-net in satellite images for residential panels, achieving 74% IoU. Recently, Jie et al. [82] combined a U-net model with edge detection networks. The authors showed that the edge detection increased performance on two city panel datasets by nearly 2% IoU. This effect may be even less prominent in large solar plants since it is easier to detect borders, as shown in our study. Even though these studies trained with smaller PV solar panels, the results show an excellent ability to segment panels even with simpler models.

Thus, the results of our and previous studies suggest that the mapping of PV solar panels should be addressed in a data-driven, rather than model-driven, perspective, i.e., the DL models do not present a significant difference, and the most important endeavor is to obtain a reliable source of generating good annotations. Moreover, the present study showed significant results using data augmentation despite a limited amount of data.

The mosaicking procedure enables the classification of areas of indefinite and large sizes. We have shown that using a smaller stride value increases performance, but also the computational cost. The stride value for a practical application should take both factors into consideration. Regarding the mosaicking technique on semantic segmentation models, de Albuquerque et al. [86] performed a comparative analysis using different stride values, presenting progressively better ROC AUC scores for lower stride values, a result also verified in our research.

This research presents many possibilities for future studies. A first proposition would be to estimate energy production using the mapping of the photovoltaic solar panel from DL, and the level of solar incidence in a specific region. Another relevant test would be evaluating radar images due to cloud cover and atmospheric interference in optical images. Although synthetic aperture radar (SAR) images are noisy, they can be useful in some scenarios. Studies comparing the frame sizes according to the proposal by Bem et al. [102] can also be valuable in understanding the model's differences in various tasks (e.g., binary and multiclass) and object scales.

5. Conclusions

The survey and monitoring of PV solar power plants are extremely important for energy management and planning. The high growth of solar energy in Brazil, a country with continental dimensions, generates an increase in inspection processes for ANEEL that is only possible through technological innovation. Thus, this paper presented a comparison between DL models for the classification of PV solar plants using Sentinel-2 images with four spectral bands (RGB and near infra-red), comparing four architectures

(U-net, DeepLabv3+, FPN, and PSPNet) with four backbones (ResNet-50, ResNet-101, Eff-b0, and Eff-b7), totaling 16 combinations. Additionally, we used augmentation and transfer learning. The PV panel spectral and shape characteristics facilitate the accurate detection of the panels. Results were satisfactory using the different backbones and architectures, but U-net with Eff-b7 backbone presented the best results with 98% accuracy, 92% IoU, and 95% F-score. We estimate that the most critical factors when mapping PV solar panels are a reliable source of data and their possible applications. For the classification of large regions, the image mosaicking procedure significantly improves when using more overlapping pixels, minimizing edge errors. The results are also expressive when analyzing the ROC AUC score and PR AUC score, in which the results progressively increase whilst decreasing the stride value. However, the computational cost may be a significant challenge for practical applications, since the processing time significantly increases with the stride value reduction. This methodology has many applications and satisfies the conditions for automatically classifying PV solar plants using free Sentinel-2 imagery, allowing for a significant advance in monitoring the implanted infrastructure.

Author Contributions: Conceptualization, M.V.C.V.d.C., O.L.F.d.C., A.G.O., and I.H.; methodology, O.L.F.d.C., O.A.d.C.J., and A.O.d.A.; software, O.L.F.d.C.; validation, M.V.C.V.d.C., A.O.d.A., and F.V.e.S.; formal analysis, O.L.F.d.C., O.A.d.C.J., and R.F.G.; investigation, M.V.C.V.d.C. and O.L.F.d.C.; resources, A.G.O., I.H., O.A.d.C.J., R.A.T.G., and R.F.G.; data curation, O.L.F.d.C., A.O.d.A., and F.V.e.S.; writing—original draft preparation, M.V.C.V.d.C., O.L.F.d.C., and O.A.d.C.J.; writing—review and editing, M.V.C.V.d.C., O.L.F.d.C., R.F.G., and O.A.d.C.J.; supervision, A.G.O., I.H., R.A.T.G., and R.F.G.; project administration, A.G.O., I.H., R.A.T.G., and R.F.G.; funding acquisition, A.G.O., I.H., R.A.T.G., R.F.G, and O.A.d.C.J. All authors have read and agreed to the published version of the manuscript.

Funding: This research was funded by the following institutions: National Council for Scientific and Technological Development (434838/2018-7) and Coordination for the Improvement of Higher Education Personnel (Finance Code 001).

Institutional Review Board Statement: Not applicable.

Informed Consent Statement: Not applicable.

Data Availability Statement: The following research materials are available online at https://github.com/osmarluiz/large-scale-solar-panel (accessed on 12 May 2021).

Acknowledgments: The authors are grateful for financial support from CNPq fellowship (Osmar Abílio de Carvalho Júnior, Roberto Arnaldo Trancoso Gomes, and Renato Fontes Guimarães). Special thanks are given to the research group of the Laboratory of Spatial Information System of the University of Brasilia for technical support. The authors thank the researchers from the ANEEL, who encouraged research with deep learning. Finally, the authors acknowledge the contribution of anonymous reviewers.

Conflicts of Interest: The authors declare no conflict of interest.

References

1. Kabir, E.; Kumar, P.; Kumar, S.; Adelodun, A.A.; Kim, K.H. Solar energy: Potential and future prospects. *Renew. Sustain. Energy Rev.* **2018**, *82*, 894–900. [CrossRef]
2. Subtil Lacerda, J.; Van Den Bergh, J.C.J.M. Diversity in solar photovoltaic energy: Implications for innovation and policy. *Renew. Sustain. Energy Rev.* **2016**, *54*, 331–340. [CrossRef]
3. Sampaio, P.G.V.; González, M.O.A. Photovoltaic solar energy: Conceptual framework. *Renew. Sustain. Energy Rev.* **2017**, *74*, 590–601. [CrossRef]
4. Jäger-Waldau, A. Snapshot of photovoltaics-February 2020. *Energies* **2020**, *13*, 930. [CrossRef]
5. Rabaia, M.K.H.; Abdelkareem, M.A.; Sayed, E.T.; Elsaid, K.; Chae, K.J.; Wilberforce, T.; Olabi, A.G. Environmental impacts of solar energy systems: A review. *Sci. Total Environ.* **2021**, *754*, 141989. [CrossRef]
6. IPCC Painel Intergovernamental onClimate Change. *Climate Change 2014: Mitigation of Climate Change. Contribution of Working Group III to the Fifth Assessment Report of the Intergovernmental Panel on Climate Change*; Edenhofer, O., Pichs-Madruga, R., Sokona, Y., Farahani, E., Kadner, S., Seyboth, K., Adler, A., Baum, I., Brunner, S., Eickemeier, P., et al., Eds.; Cambridge University Press: Cambridge, UK, 2014; ISBN 9781107654815. [CrossRef]

7. Creutzig, F.; Agoston, P.; Goldschmidt, J.C.; Luderer, G.; Nemet, G.; Pietzcker, R.C. The underestimated potential of solar energy to mitigate climate change. *Nat. Energy* **2017**, *2*. [CrossRef]
8. Gils, H.C.; Simon, S.; Soria, R. 100% Renewable energy supply for Brazil-The role of sector coupling and regional development. *Energies* **2017**, *10*, 1859. [CrossRef]
9. Mendes, L.F.R.; Sthel, M.S. Analysis of the hydrological cycle and its impacts on the sustainability of the electric matrix in the state of Rio de Janeiro/Brazil. *Energy Strateg. Rev.* **2018**, *22*, 119–126. [CrossRef]
10. Mendes, L.F.R.; Sthel, M.S. Thermoelectric Power Plant for Compensation of Hydrological Cycle Change: Environmental Impacts in Brazil. *Case Stud. Environ.* **2017**, *1*, 1–7. [CrossRef]
11. Melo, L.B.; Estanislau, F.B.G.L.E.; Costa, A.L.; Fortini, Â. Impacts of the hydrological potential change on the energy matrix of the Brazilian State of Minas Gerais: A case study. *Renew. Sustain. Energy Rev.* **2019**, *110*, 415–422. [CrossRef]
12. Reichert, B.; Souza, A.M. Interrelationship simulations among Brazilian electric matrix sources. *Electr. Power Syst. Res.* **2021**, *193*, 107019. [CrossRef]
13. Athayde, S.; Mathews, M.; Bohlman, S.; Brasil, W.; Doria, C.R.; Dutka-Gianelli, J.; Fearnside, P.M.; Loiselle, B.; Marques, E.E.; Melis, T.S.; et al. Mapping research on hydropower and sustainability in the Brazilian Amazon: Advances, gaps in knowledge and future directions. *Curr. Opin. Environ. Sustain.* **2019**, *37*, 50–69. [CrossRef]
14. Manyari, W.V.; de Carvalho, O.A. Environmental considerations in energy planning for the Amazon region: Downstream effects of dams. *Energy Policy* **2007**, *35*, 6526–6534. [CrossRef]
15. Latrubesse, E.M.; Arima, E.Y.; Dunne, T.; Park, E.; Baker, V.R.; D'Horta, F.M.; Wight, C.; Wittmann, F.; Zuanon, J.; Baker, P.A.; et al. Damming the rivers of the Amazon basin. *Nature* **2017**, *546*, 363–369. [CrossRef] [PubMed]
16. De Faria, F.A.M.; Jaramillo, P. The future of power generation in Brazil: An analysis of alternatives to Amazonian hydropower development. *Energy Sustain. Dev.* **2017**, *41*, 24–35. [CrossRef]
17. De Jong, P.; Barreto, T.B.; Tanajura, C.A.S.; Kouloukoui, D.; Oliveira-Esquerre, K.P.; Kiperstok, A.; Torres, E.A. Estimating the impact of climate change on wind and solar energy in Brazil using a South American regional climate model. *Renew. Energy* **2019**, *141*, 390–401. [CrossRef]
18. Ferraz de Andrade Santos, J.A.; de Jong, P.; Alves da Costa, C.; Torres, E.A. Combining wind and solar energy sources: Potential for hybrid power generation in Brazil. *Util. Policy* **2020**, *67*. [CrossRef]
19. Ferreira, A.; Kunh, S.S.; Fagnani, K.C.; De Souza, T.A.; Tonezer, C.; Dos Santos, G.R.; Coimbra-Araújo, C.H. Economic overview of the use and production of photovoltaic solar energy in brazil. *Renew. Sustain. Energy Rev.* **2018**, *81*, 181–191. [CrossRef]
20. Martins, F.R.; Abreu, S.L.; Pereira, E.B. Scenarios for solar thermal energy applications in Brazil. *Energy Policy* **2012**, *48*, 640–649. [CrossRef]
21. Martins, F.R.; Rüther, R.; Pereira, E.B.; Abreu, S.L. Solar energy scenarios in Brazil. Part two: Photovoltaics applications. *Energy Policy* **2008**, *36*, 2865–2877. [CrossRef]
22. Martins, F.R.; Pereira, E.B.; Silva, S.A.B.; Abreu, S.L.; Colle, S. Solar energy scenarios in Brazil, Part one: Resource assessment. *Energy Policy* **2008**, *36*, 2853–2864. [CrossRef]
23. De Lima, F.J.L.; Martins, F.R.; Costa, R.S.; Gonçalves, A.R.; dos Santos, A.P.P.; Pereira, E.B. The seasonal variability and trends for the surface solar irradiation in northeastern region of Brazil. *Sustain. Energy Technol. Assess.* **2019**, *35*, 335–346. [CrossRef]
24. Azevêdo, V.W.B.; Candeias, L.B.; Tiba, C. Location study of solar thermal power plant in the state of Pernambuco using geoprocessing technologies and Multiple-Criteria analysis. *Energies* **2017**, *10*, 1042. [CrossRef]
25. Medeiros, S.E.L.; Nilo, P.F.; Silva, L.P.; Santos, C.A.C.; Carvalho, M.; Abrahão, R. Influence of climatic variability on the electricity generation potential by renewable sources in the Brazilian semi-arid region. *J. Arid Environ.* **2021**, *184*, 104331. [CrossRef]
26. Vieira de Souza, L.E.; Gilmanova Cavalcante, A.M. Concentrated Solar Power deployment in emerging economies: The cases of China and Brazil. *Renew. Sustain. Energy Rev.* **2017**, *72*, 1094–1103. [CrossRef]
27. De Faria, H.; Trigoso, F.B.M.; Cavalcanti, J.A.M. Review of distributed generation with photovoltaic grid connected systems in Brazil: Challenges and prospects. *Renew. Sustain. Energy Rev.* **2017**, *75*, 469–475. [CrossRef]
28. Amaral, A.B.A.; Mendonca, A.L.Z.L.G.; Resende, A.A.M.; Rego, E.E. Solar energy and distributed generation: 2015, a year of inflection in Brazil? *IEEE Lat. Am. Trans.* **2016**, *14*, 3731–3737. [CrossRef]
29. Elgamal, G.N.G.; Demajorovic, J. Barriers and perspectives for electric power generation out of photovoltaic solar panels in the brazilian energy matrix. *Rev. Gest. Ambient. Sustent.* **2020**, *9*, 1–26. [CrossRef]
30. Garlet, T.B.; Ribeiro, J.L.D.; de Souza Savian, F.; Mairesse Siluk, J.C. Paths and barriers to the diffusion of distributed generation of photovoltaic energy in southern Brazil. *Renew. Sustain. Energy Rev.* **2019**, *111*, 157–169. [CrossRef]
31. Vilaça Gomes, P.; Knak Neto, N.; Carvalho, L.; Sumaili, J.; Saraiva, J.T.; Dias, B.H.; Miranda, V.; Souza, S.M. Technical-economic analysis for the integration of PV systems in Brazil considering policy and regulatory issues. *Energy Policy* **2018**, *115*, 199–206. [CrossRef]
32. Hoffmann, A.S.; de Carvalho, G.H.; Cardoso, R.A.F. Environmental licensing challenges for the implementation of photovoltaic solar energy projects in Brazil. *Energy Policy* **2019**, *132*, 1143–1154. [CrossRef]
33. Queiroz, J.V.; Borges, K.K.; Queiroz, F.C.B.P.; Lima, N.C.; Da Silva, C.L.; de Souza Morais, L. Barriers to expand solar photovoltaic energy in Brazil. *Indep. J. Manag. Prod.* **2020**, *11*, 2733–2754. [CrossRef]
34. Denes_Santos, D.; da Cunha, S.K. Transformative innovation policy for solar energy: Particularities of a developing country. *Clean Technol. Environ. Policy* **2020**, *22*, 43–57. [CrossRef]

35. Barbosa, J.; Dias, L.P.; Simoes, S.G.; Seixas, J. When is the sun going to shine for the Brazilian energy sector? A story of how modelling affects solar electricity. *Renew. Energy* **2020**, *162*, 1684–1702. [CrossRef]
36. Viana, A.G.; Ramos, D.S. Outcomes from the first large-scale solar PV auction in Brazil. *Renew. Sustain. Energy Rev.* **2018**, *91*, 219–228. [CrossRef]
37. Echegaray, F. Understanding stakeholders' views and support for solar energy in Brazil. *J. Clean. Prod.* **2014**, *63*, 125–133. [CrossRef]
38. Orlandi, A.G.; Farias, R.A.N.; de Carvalho Junior, O.A.; Guimarães, R.F.; Gomes, R.A.T. Controle gerencial na administração pública e transformação digital: Sensoriamento remoto. *Cad. Gestão Pública Cid.* **2021**, *26*, 1–24. [CrossRef]
39. Deng, C.; Wang, S.; Huang, Z.; Tan, Z.; Liu, J. Unmanned aerial vehicles for power line inspection: A cooperative way in platforms and communications. *J. Commun.* **2014**, *9*, 687–692. [CrossRef]
40. Matikainen, L.; Lehtomäki, M.; Ahokas, E.; Hyyppä, J.; Karjalainen, M.; Jaakkola, A.; Kukko, A.; Heinonen, T. Remote sensing methods for power line corridor surveys. *ISPRS J. Photogramm. Remote Sens.* **2016**, *119*, 10–31. [CrossRef]
41. Ahmad, J.; Malik, A.S.; Xia, L.; Ashikin, N. Vegetation encroachment monitoring for transmission lines right-of-ways: A survey. *Electr. Power Syst. Res.* **2013**, *95*, 339–352. [CrossRef]
42. Bonansea, M.; Ferrero, S.; Ferral, A.; Ledesma, M.; German, A.; Carreño, J.; Rodriguez, C.; Pinotti, L. Assessing water surface temperature from Landsat imagery and its relationship with a nuclear power plant. *Hydrol. Sci. J.* **2021**, *66*, 50–58. [CrossRef]
43. Ma, P.; Dai, X.; Guo, Z.; Wei, C.; Ma, W. Detection of thermal pollution from power plants on China's eastern coast using remote sensing data. *Stoch. Environ. Res. Risk Assess.* **2017**, *31*, 1957–1975. [CrossRef]
44. Ahn, Y.H.; Shanmugam, P.; Lee, J.H.; Kang, Y.Q. Application of satellite infrared data for mapping of thermal plume contamination in coastal ecosystem of Korea. *Mar. Environ. Res.* **2006**, *61*, 186–201. [CrossRef] [PubMed]
45. Chen, C.; Shi, P.; Mao, Q. Application of remote sensing techniques for monitoring the thermal pollution of cooling-water discharge from nuclear power plant. *J. Environ. Sci. Health Part A Toxic Hazard. Subst. Environ. Eng.* **2003**, *38*, 1659–1668. [CrossRef] [PubMed]
46. Bauni, V.; Schivo, F.; Capmourteres, V.; Homberg, M. Ecosystem loss assessment following hydroelectric dam flooding: The case of Yacyretá, Argentina. *Remote Sens. Appl. Soc. Environ.* **2015**, *1*, 50–60. [CrossRef]
47. Chen, G.; Powers, R.P.; de Carvalho, L.M.T.; Mora, B. Spatiotemporal patterns of tropical deforestation and forest degradation in response to the operation of the Tucuruí hydroelectricdam in the Amazon basin. *Appl. Geogr.* **2015**, *63*, 1–8. [CrossRef]
48. Jiang, X.; Lu, D.; Moran, E.; Calvi, M.F.; Dutra, L.V.; Li, G. Examining impacts of the Belo Monte hydroelectric dam construction on land-cover changes using multitemporal Landsat imagery. *Appl. Geogr.* **2018**, *97*, 35–47. [CrossRef]
49. Feng, L.; Hu, C.; Chen, X.; Zhao, X. Dramatic inundation changes of China's two largest freshwater lakes linked to the Three Gorges Dam. *Environ. Sci. Technol.* **2013**, *47*, 9628–9634. [CrossRef] [PubMed]
50. Beyer, R.C.M.; Franco-Bedoya, S.; Galdo, V. Examining the economic impact of COVID-19 in India through daily electricity consumption and nighttime light intensity. *World Dev.* **2021**, *140*, 105287. [CrossRef]
51. Dugoua, E.; Kennedy, R.; Urpelainen, J. Satellite data for the social sciences: Measuring rural electrification with night-time lights. *Int. J. Remote Sens.* **2018**, *39*, 2690–2701. [CrossRef]
52. Min, B.; Gaba, K.M. Tracking electrification in Vietnam using nighttime lights. *Remote Sens.* **2014**, *6*, 9511–9529. [CrossRef]
53. Hammer, A.; Heinemann, D.; Hoyer, C.; Kuhlemann, R.; Lorenz, E.; Müller, R.; Beyer, H.G. Solar energy assessment using remote sensing technologies. *Remote Sens. Environ.* **2003**, *86*, 423–432. [CrossRef]
54. Yang, D.; Kleissl, J.; Gueymard, C.A.; Pedro, H.T.C.; Coimbra, C.F.M. History and trends in solar irradiance and PV power forecasting: A preliminary assessment and review using text mining. *Sol. Energy* **2018**, *168*, 60–101. [CrossRef]
55. Masoom, A.; Kosmopoulos, P.; Bansal, A.; Kazadzis, S. Solar energy estimations in india using remote sensing technologies and validation with sun photometers in urban areas. *Remote Sens.* **2020**, *12*, 254. [CrossRef]
56. Kausika, B.; van Sark, W. Calibration and Validation of ArcGIS Solar Radiation Tool for Photovoltaic Potential Determination in the Netherlands. *Energies* **2021**, *14*, 1865. [CrossRef]
57. Al Garni, H.Z.; Awasthi, A. Solar PV Power Plants Site Selection: A Review. In *Advances in Renewable Energies and Power Technologies*; Yahyaoui, I., Ed.; Elsevier Inc.: Amsterdam, The Netherlands, 2018; Volume 1, pp. 57–75, ISBN 9780128132173.
58. Gherboudj, I.; Ghedira, H. Assessment of solar energy potential over the United Arab Emirates using remote sensing and weather forecast data. *Renew. Sustain. Energy Rev.* **2016**, *55*, 1210–1224. [CrossRef]
59. Mahtta, R.; Joshi, P.K.; Jindal, A.K. Solar power potential mapping in India using remote sensing inputs and environmental parameters. *Renew. Energy* **2014**, *71*, 255–262. [CrossRef]
60. Polo, J.; Bernardos, A.; Navarro, A.A.; Fernandez-Peruchena, C.M.; Ramírez, L.; Guisado, M.V.; Martínez, S. Solar resources and power potential mapping in Vietnam using satellite-derived and GIS-based information. *Energy Convers. Manag.* **2015**, *98*, 348–358. [CrossRef]
61. Wang, S.; Zhang, L.; Fu, D.; Lu, X.; Wu, T.; Tong, Q. Selecting photovoltaic generation sites in Tibet using remote sensing and geographic analysis. *Sol. Energy* **2016**, *133*, 85–93. [CrossRef]
62. Spyridonidou, S.; Sismani, G.; Loukogeorgaki, E.; Vagiona, D.G.; Ulanovsky, H.; Madar, D. Sustainable Spatial Energy Planning of Large-Scale Wind and PV Farms in Israel: A Collaborative and Participatory Planning Approach. *Energies* **2021**, *14*, 551. [CrossRef]

63. Sánchez-Aparicio, M.; Del Pozo, S.; Martín-Jiménez, J.A.; González-González, E.; Andrés-Anaya, P.; Lagüela, S. Influence of lidar point cloud density in the geometric characterization of rooftops for solar photovoltaic studies in cities. *Remote Sens.* **2020**, *12*, 3726. [CrossRef]
64. Tiwari, A.; Meir, I.A.; Karnieli, A. Object-based image procedures for assessing the solar energy photovoltaic potential of heterogeneous rooftops using airborne LiDAR and orthophoto. *Remote Sens.* **2020**, *12*, 223. [CrossRef]
65. Prieto, I.; Izkara, J.L.; Usobiaga, E. The application of LiDAR data for the solar potential analysis based on urban 3D model. *Remote Sens.* **2019**, *11*, 2348. [CrossRef]
66. Li, Y.; Liu, C. Estimating solar energy potentials on pitched roofs. *Energy Build.* **2017**, *139*, 101–107. [CrossRef]
67. Karoui, M.S.; Benhalouche, F.Z.; Deville, Y.; Djerriri, K.; Briottet, X.; Houet, T.; Le Bris, A.; Weber, C. Partial linear NMF-based unmixing methods for detection and area estimation of photovoltaic panels in urban hyperspectral remote sensing data. *Remote Sens.* **2019**, *11*, 2164. [CrossRef]
68. Malof, J.M.; Bradbury, K.; Collins, L.M.; Newell, R.G. Automatic detection of solar photovoltaic arrays in high resolution aerial imagery. *Appl. Energy* **2016**, *183*, 229–240. [CrossRef]
69. Lecun, Y.; Bengio, Y.; Hinton, G. Deep learning. *Nature* **2015**, *521*, 436–444. [CrossRef]
70. Ball, J.E.; Anderson, D.T.; Chan, C.S. Special Section Guest Editorial: Feature and Deep Learning in Remote Sensing Applications. *J. Appl. Remote Sens.* **2018**, *11*, 1. [CrossRef]
71. Maxwell, A.E.; Warner, T.A.; Fang, F. Implementation of machine-learning classification in remote sensing: An applied review. *Int. J. Remote Sens.* **2018**, *39*, 2784–2817. [CrossRef]
72. Yuan, Q.; Shen, H.; Li, T.; Li, Z.; Li, S.; Jiang, Y.; Xu, H.; Tan, W.; Yang, Q.; Wang, J.; et al. Deep learning in environmental remote sensing: Achievements and challenges. *Remote Sens. Environ.* **2020**, *241*, 111716. [CrossRef]
73. Zhang, L.; Zhang, L.; Du, B. Deep Learning for Remote Sensing Data: A Technical Tutorial on the State of the Art. *IEEE Geosci. Remote Sens. Mag.* **2016**, *4*, 22–40. [CrossRef]
74. Ma, L.; Liu, Y.; Zhang, X.; Ye, Y.; Yin, G.; Johnson, B.A. Deep learning in remote sensing applications: A meta-analysis and review. *ISPRS J. Photogramm. Remote Sens.* **2019**, *152*, 166–177. [CrossRef]
75. Zhu, X.X.; Tuia, D.; Mou, L.; Xia, G.; Zhang, L.; Xu, F.; Fraundorfer, F. Deep Learning in Remote Sensing: A Comprehensive Review and List of Resources. *IEEE Geosci. Remote Sens. Mag.* **2017**, *5*, 8–36. [CrossRef]
76. Garcia-Garcia, A.; Orts-Escolano, S.; Oprea, S.; Villena-Martinez, V.; Martinez-Gonzalez, P.; Garcia-Rodriguez, J. A survey on deep learning techniques for image and video semantic segmentation. *Appl. Soft Comput.* **2018**, *70*, 41–65. [CrossRef]
77. Guo, Y.; Liu, Y.; Oerlemans, A.; Lao, S.; Wu, S.; Lew, M.S. Deep learning for visual understanding: A review. *Neurocomputing* **2016**, *187*, 27–48. [CrossRef]
78. Liu, L.; Ouyang, W.; Wang, X.; Fieguth, P.; Chen, J.; Liu, X.; Pietikäinen, M. Deep learning for generic object detection: A survey. *Int. J. Comput. Vis.* **2020**, *128*, 261–318. [CrossRef]
79. Yu, H.; Yang, Z.; Tan, L.; Wang, Y.; Sun, W.; Sun, M.; Tang, Y. Methods and datasets on semantic segmentation: A review. *Neurocomputing* **2018**, *304*, 82–103. [CrossRef]
80. Lateef, F.; Ruichek, Y. Survey on semantic segmentation using deep learning techniques. *Neurocomputing* **2019**, *338*, 321–348. [CrossRef]
81. Bradbury, K.; Saboo, R.; Johnson, T.L.; Malof, J.M.; Devarajan, A.; Zhang, W.; Collins, L.M.; Newell, R.G. Distributed solar photovoltaic array location and extent dataset for remote sensing object identification. *Sci. Data* **2016**, *3*, 1–9. [CrossRef]
82. Jie, Y.; Ji, X.; Yue, A.; Chen, J.; Deng, Y.; Chen, J.; Zhang, Y. Combined Multi-Layer Feature Fusion and Edge Detection Method for Distributed Photovoltaic Power Station Identification. *Energies* **2020**, *13*, 6742. [CrossRef]
83. Zhuang, L.; Zhang, Z.; Wang, L. The automatic segmentation of residential solar panels based on satellite images: A cross learning driven U-Net method. *Appl. Soft Comput. J.* **2020**, *92*, 106283. [CrossRef]
84. Hou, X.; Wang, B.; Hu, W.; Yin, L.; Wu, H. SolarNet: A Deep Learning Framework to Map Solar Power Plants In China From Satellite Imagery. *arXiv* **2019**, arXiv:1912.03685.
85. Audebert, N.; Boulch, A.; Randrianarivo, H.; Le, B.; Ferecatu, M.; Lefèvre, S.; Marlet, R.; Audebert, N.; Boulch, A.; Randrianarivo, H.; et al. Deep learning for urban remote sensing. In Proceedings of the Joint Urban Remote Sensing Event (JURSE), Dubai, United Arab Emirates, 6–8 March 2017; p. Hal-01672854. [CrossRef]
86. De Albuquerque, A.O.; de Carvalho Júnior, O.A.A.; de Carvalho, O.L.F.; de Bem, P.P.; Ferreira, P.H.G.; dos Santos de Moura, R.; Silva, C.R.; Trancoso Gomes, R.A.; Fontes Guimarães, R. Deep Semantic Segmentation of Center Pivot Irrigation Systems from Remotely Sensed Data. *Remote Sens.* **2020**, *12*, 2159. [CrossRef]
87. De Carvalho, O.L.F.; de Carvalho Júnior, O.A.A.; de Albuquerque, A.O.; de Bem, P.P.; Silva, C.R.; Ferreira, P.H.G.; dos Santos de Moura, R.; Gomes, R.A.T.; Guimarães, R.F.; Borges, D.L.D.L. Instance Segmentation for Large, Multi-Channel Remote Sensing Imagery Using Mask-RCNN and a Mosaicking Approach. *Remote Sens.* **2021**, *13*, 39. [CrossRef]
88. Drusch, M.; Del Bello, U.; Carlier, S.; Colin, O.; Fernandez, V.; Gascon, F.; Hoersch, B.; Isola, C.; Laberinti, P.; Martimort, P.; et al. Sentinel-2: ESA's Optical High-Resolution Mission for GMES Operational Services. *Remote Sens. Environ.* **2012**, *120*, 25–36. [CrossRef]
89. Ronneberger, O.; Fischer, P.; Brox, T. U-Net: Convolutional Networks for Biomedical Image Segmentation. In *Lecture Notes in Computer Science*; Including subseries Lecture Notes in Artificial Intelligence and Lecture Notes in Bioinformatics; Navab, N., Hornegger, J., Wells, W., Frangi, A., Eds.; Springer: Cham, Switzerland, 2015; Volume 9351, pp. 234–241, ISBN 9783319245737.

90. Badrinarayanan, V.; Kendall, A.; Cipolla, R. SegNet: A Deep Convolutional Encoder-Decoder Architecture for Image Segmentation. *IEEE Trans. Pattern Anal. Mach. Intell.* **2017**, *39*, 2481–2495. [CrossRef]
91. Lin, T.-Y.; Dollar, P.; Girshick, R.; He, K.; Hariharan, B.; Belongie, S. Feature Pyramid Networks for Object Detection. In Proceedings of the 2017 IEEE Conference on Computer Vision and Pattern Recognition (CVPR), Honolulu, HI, USA, 21–26 July 2017; pp. 936–944.
92. Chen, L.-C.; Papandreou, G.; Kokkinos, I.; Murphy, K.; Yuille, A.L. DeepLab: Semantic Image Segmentation with Deep Convolutional Nets, Atrous Convolution, and Fully Connected CRFs. *IEEE Trans. Pattern Anal. Mach. Intell.* **2018**, *40*, 834–848. [CrossRef] [PubMed]
93. Chen, L.-C.; Zhu, Y.; Papandreou, G.; Schroff, F.; Adam, H. Encoder-Decoder with Atrous Separable Convolution for Semantic Image Segmentation. *Pertanika J. Trop. Agric. Sci.* **2018**, *34*, 137–143.
94. Zhao, H.; Shi, J.; Qi, X.; Wang, X.; Jia, J. Pyramid Scene Parsing Network. In Proceedings of the 2017 IEEE Conference on Computer Vision and Pattern Recognition (CVPR), Honolulu, HI, USA, 21–26 July 2017; pp. 6230–6239.
95. He, K.; Zhang, X.; Ren, S.; Sun, J. Deep Residual Learning for Image Recognition. In Proceedings of the 2016 IEEE Conference on Computer Vision and Pattern Recognition (CVPR), Las Vegas, NV, USA, 27–30 June 2016; Volume 45, pp. 770–778.
96. Xie, S.; Girshick, R.; Dollar, P.; Tu, Z.; He, K. Aggregated Residual Transformations for Deep Neural Networks. In Proceedings of the 2017 IEEE Conference on Computer Vision and Pattern Recognition (CVPR), Honolulu, HI, USA, 21–26 July 2017; pp. 5987–5995.
97. Tan, M.; Le, Q.V. EfficientNet: Rethinking Model Scaling for Convolutional Neural Networks. *arXiv* **2019**, arXiv:1905.11946.
98. Yakubovskiy, P. Segmentation Models Pytorch. GitHub Repos. 2020. Available online: https://github.com/qubvel/segmentation_models.pytorch (accessed on 14 April 2021).
99. Deng, J.; Dong, W.; Socher, R.; Li, L.-J.; Li, K.; Li, F.-F. ImageNet: A large-scale hierarchical image database. In Proceedings of the 2009 IEEE Conference on Computer Vision and Pattern Recognition, Miami, FL, USA, 20–25 June 2009; pp. 248–255.
100. Yuan, J.; Yang, H.H.L.; Omitaomu, O.A.; Bhaduri, B.L. Large-scale solar panel mapping from aerial images using deep convolutional networks. In Proceedings of the 2016 International Conference on Big Data, Washington, DC, USA, 5–8 December 2016; pp. 2703–2708. [CrossRef]
101. Yu, J.; Wang, Z.; Majumdar, A.; Rajagopal, R. DeepSolar: A Machine Learning Framework to Efficiently Construct a Solar Deployment Database in the United States. *Joule* **2018**, *2*, 2605–2617. [CrossRef]
102. De Bem, P.P.; de Carvalho Júnior, O.A.; de Carvalho, O.L.F.; Gomes, R.A.T.; Fontes Guimarães, R.; Guimarães, R.F. Performance Analysis of Deep Convolutional Autoencoders with Different Patch Sizes for Change Detection from Burnt Areas. *Remote Sens.* **2020**, *12*, 2576. [CrossRef]